Petroleum Science
https://doi.org/10.1007/s12182-021-00558-x

ORIGINAL PAPER

EDTA interfacial chelation Ca^{2+} incorporates superhydrophobic coating for scaling inhibition of $CaCO_3$ in petroleum industry

Ming-Liang Zhu[1] · Hui-Juan Qian[1,2] · Rui-Xia Yuan[1] · Dong-Yan Zhao[3] · Hai-Chao Huang[3] · Huai-Yuan Wang[1]

Received: 16 November 2020 / Accepted: 5 January 2021

Abstract
In this paper, the superhydrophobic poly(vinylidene fluoride)/fluorinated ethylene propylene/SiO_2/CNTs-EDTA (PFSC-EDTA) composite coating was successfully fabricated and applied for anti-scaling performance. The deposition of $CaCO_3$ on the surface of the superhydrophobic PFSC-EDTA composite coating reached 0.0444 mg/cm^2 for 192-h immersion into the supersaturated $CaCO_3$ solution, which was only 11.4% that of the superhydrophobic PFSC composite coating. At the interface between the $CaCO_3$ solution and the PFSC-EDTA coating, the Ca^{2+} could be firstly chelated by EDTA that was benefit for improving the anti-scaling performance of the superhydrophobic PFSC-EDTA composite coating. In another hand, the addition of EDTA to the CNTs played an important role in fabricating the SiO_2-centric and CNTs-EDTA-surrounded multilevel micro–nanostructure in the superhydrophobic PFSC-EDTA composite coating, in favor of maintaining the air film under the water and the stability of the superhydrophobic surface. The research supplies a new way of improving anti-scaling performance of superhydrophobic coating by incorporating the organic chelating agent at the interface and changing the traditional way of scale prevention.

Keywords Anti-scaling · Superhydrophobic coating · EDTA · Poly(vinylidene fluoride) · Carbon nanotubes

1 Introduction

Scaling is very common in the petroleum industry, heat exchangers, high-power heat sinks and electronics and the corresponded industries especially in the process of oil exploitation. The formation of scale is due to the precipitation of inorganic salts such as calcium carbonate, calcium sulfate and magnesium hydroxide. The scale in the pipeline will narrow the area of cross section conduits, increase the flow resistance of fluid and reduce the transportation efficiency (Vazirian et al. 2016; Wang et al. 2019a; Liu et al. 2019). The pipeline will be completely blocked in serious cases, which may affect the normal production of the oilfield (Wang et al. 2019b). Therefore, people pay more attention to the anti-scaling technology and materials. The chemical method for scale prevention is widely used in petroleum industry, that the chemical anti-scaling agent was poured into the liquid to be treated by binding with the divalent cations such as Ca^{2+}, Mg^{2+}, Ba^{2+} and so on. At present, the commonly used commercial-scale inhibitor includes ethylenediaminetetraacetic acid (EDTA), diethylenetriamine pentaacetic acid (DTPA), ethylenediaminetetramethylene phosphonic acid (EDTMP), aminotrimethylene phosphonic acid (ATMP) and 1-hydroxyethylidene-1, 1-diphosphonic acid (HEDP) (Khormali and Petrakov 2016). These scale inhibitors can not only form complexes with Ca^{2+}/Mg^{2+} and reduce supersaturation level, but also weak their adhesion to the surface due to their morphological dissymmetry (Mpelwa and Tang 2019). Though the addition of the anti-scaling agent could inhibit the formation of scale particles in solution, the high cost and low efficiency restricted its application, especially in pipeline flow system. As a typical

Edited by Xiu-Qiu Peng

Handling Editor: Zhen-Hua Rui

✉ Huai-Yuan Wang
wanghyjiji@163.com

[1] College of Chemistry and Chemical Engineering, Northeast Petroleum University, Daqing 163318, China

[2] College of Chemical Engineering, Daqing Normal University, Daqing 163712, China

[3] Beijing Smart-Chip Microelectronics Technology Co., Ltd, Beijing 102200, China

Published online: 18 February 2021

chelant, EDTA is a kind of chelating ligand with high-affinity constant, which can form metal–EDTA complex (Mpelwa and Tang 2019; Kan et al. 2020). Because the reaction is stoichiometric, for example, one mole of EDTA can chelate two moles of Ca^{2+}. Therefore, a large number of chelators are needed for effective prevention (Mpelwa and Tang 2019). Recently, an effective and promising strategy to reduce the formation of inorganic scales has been the fabrication of anti-scaling surface by coating; among them, the pre-stored of scale inhibitors to the functional coating is one innovative idea (Zhu et al. 2021).

Due to the low surface free energy and the rough microstructure, polymer-based superhydrophobic coating with water contact angle (WCA) greater than 150° has shown its unique advantages in self-cleaning, anti-corrosion, fluid drag reduction, anti-icing and antifouling; it has become a research hot spot in many fields (Latthe et al. 2019). In our previous research, it was found that the polymer-based superhydrophobic composite coating owes excellent anti-scaling properties (Qian et al. 2017; 2020). Inspired by the anti-scaling of the polymer superhydrophobic composite coating and the chemical scale inhibitor, it is worthwhile to investigate the combination of these two ways for scale prevention. Nevertheless, there are few reports on the application of organic chelating agents to the superhydrophobic polyvinylidene fluoride (PVDF) coating and the study of $CaCO_3$ scale inhibition. The scale prevention performance of superhydrophobic PVDF composite coating was studied preliminarily (Qian et al. 2020). It is necessary to further study the deposition of $CaCO_3$ on the polymer-based superhydrophobic composite coating, coupling with the effect of organic chelating agent.

In this article, the superhydrophobic PVDF/FEP/SiO_2/CNTs-EDTA (PFSC-EDTA) composite coating was fabricated by incorporating PVDF, fluorinated ethylene propylene (FEP), nano-SiO_2 and EDTA-modified CNTs (CNTs-EDTA). The deposition of $CaCO_3$ scaling at the PFSC-EDTA coating surface was carried out at the temperature of 60 °C under the static state. The role of EDTA on the scale inhibition of the superhydrophobic PFSC-EDTA composite coating was investigated and discussed in detail. In order to understand the effect of EDTA for $CaCO_3$ scaling at the surface of superhydrophobic PFSC-EDTA composite coating, the superhydrophobic PFSC composite coating was used as a reference. Owing to the coupled effect between the organic chelating agents (EDTA) and polymer-based superhydrophobic composite coating, the PFSC-EDTA composite coating exhibits unique anti-scaling performance. This research on the organic chelating agent-enhanced anti-scaling performance of the superhydrophobic coating will play an important role in industrial application. We believe that this work will pave a new way for the anti-scaling of functional coating in petroleum industry.

2 Experimental

2.1 Materials and reagents

Commercial epoxy resin (EP, E-44) was supplied by Nanjing Huntsman Advanced Materials Co. (China). PVDF powders were bought from Shanghai 3F Co. Ltd. (China). FEP powders were purchased from DuPont, USA. The nanometer silica (SiO_2, Nanjing Hydratight Nanomaterials Co. Ltd, China) and CNTs (Beijing Boyu New Material Technology Co., Ltd, China) were used as received. Other chemical agents were all analytically pure. EDTA was bought from Tianjin No. 1 Chemical Reagent Factory. The absolute ethyl alcohol, ethyl acetate, calcium nitrate terahydrate, sodium bicarbonate, ethanediamine and ethylene glycol (EG) were all bought from Huadong Reagent Factory, Shenyang, China.

2.2 Preparation of the superhydrophobic PFSC composite coating

It is well known that the Q235 carbon steel and aluminum materials are widely used as tubing materials or substrate materials in the petroleum industry. The schematic diagram of the preparation process for superhydrophobic PFSC composite coating is shown in Fig. 1. The aluminum plate (80 mm × 80 mm × 1 mm) was firstly polished with 600-mesh silicon carbide sand grain paper for about 20 min; then, the sample was polished for 20 min by 800-mesh abrasive paper and finally polished in the same way with a 1000-mesh sand paper for another 20 min to obtain the average roughness of 0.15–0.30 μm. After that, the polished aluminum plate was cleaned with deionized water and then put into anhydrous ethanol solution for ultrasonic cleaning for 5 min to remove the dirt and grease attached at the aluminum plate surface.

2.0 g epoxy resin and 0.1 g PVDF powders were ultrasonically dispersed in 10 mL ethyl acetate to form a uniform solution. Then, 0.2 g ethylenediamine was added into the above solution and ultrasonically dispersed for 15 min. The resulting solution was sprayed on the as-treated aluminum plates as the basement layer, followed by drying at 180 °C for 20 min. The spraying pressure is 0.6 MPa. The distance between the aluminum plate and the spray gun is 18 cm. After that, 0.7 g PVDF powders, 0.3 g FEP powders, 0.05 g nano-SiO_2 particles and 0.05 g carbon nanofillers (CNTs) were ultrasonically dispersed in 10 mL of absolute ethyl alcohol for 30 min. Next, the above solution as a surface functional coating material was erupted on aluminum plate under a pressure of 0.6 MPa. In this way, the superhydrophobic PFSC composite coatings were obtained after drying at 180 °C for 90 min.

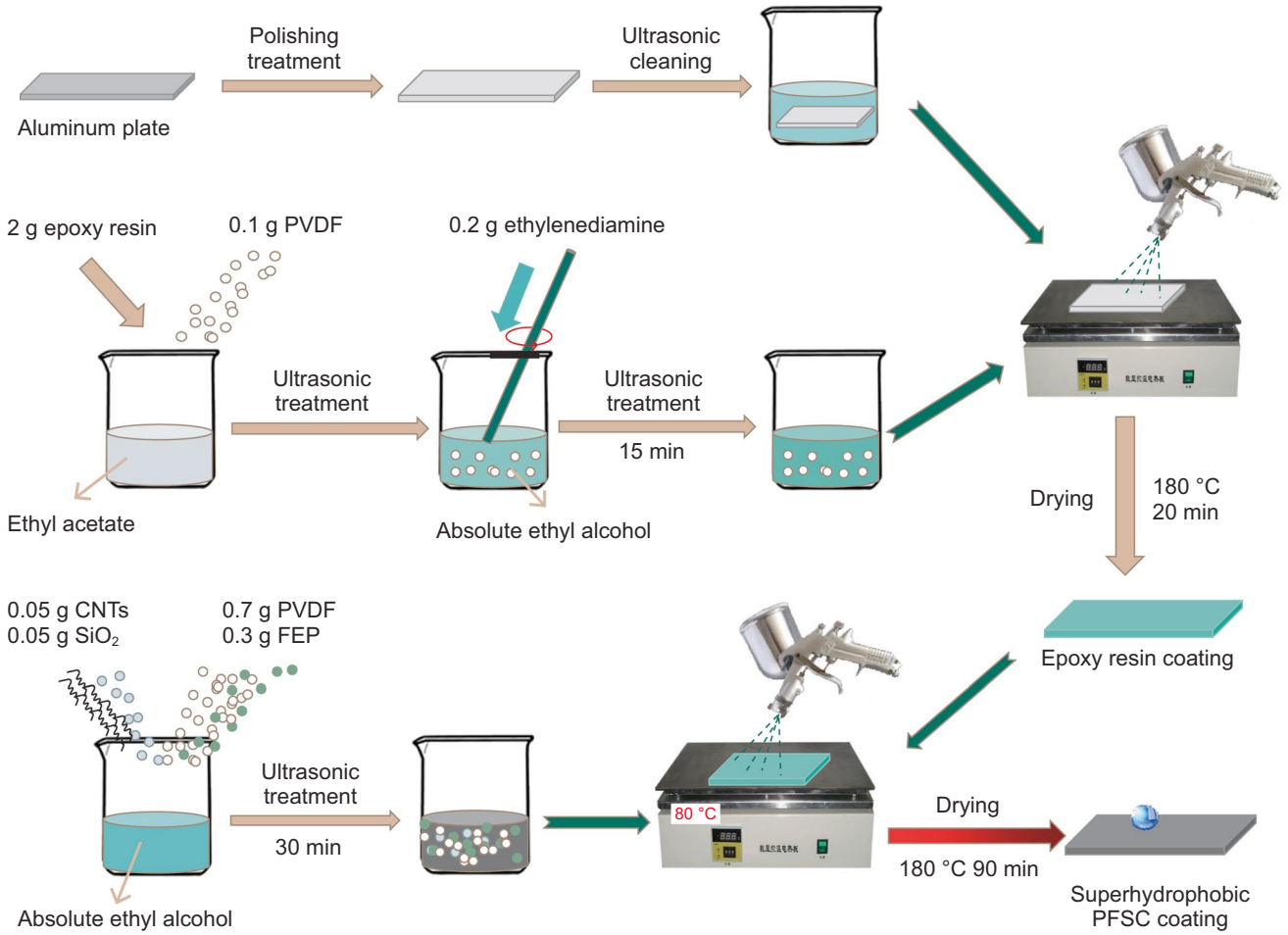

Fig. 1 Schematic diagram of the preparation process for superhydrophobic PFSC composite coating

2.3 Preparation of the superhydrophobic PFSC-EDTA composite coating

The basement layer of the PFSC-EDTA composite coating was the same as that of the PFSC composite coating. More concretely, 0.1 g CNTs were added to an organic chelating agent EDTA solution at a concentration of 0.1009 mol/L for ultrasonic impregnation. The time for EDTA and CNTs impregnation was 12 h. Then, the reaction suspension was filtered and separated. CNTs impregnated with EDTA (CNTs-EDTA) were dried in a constant temperature blast drying oven at 100–105 °C for 3 h to constant weight. Besides, 0.7 g PVDF powders, 0.3 g FEP powders, 0.05 g nano-SiO_2 particles and 0.05 g CNTs-EDTA were ultrasonically dispersed in 10 mL of absolute ethyl alcohol for 30 min. Next, as the surface functional coating material, the above solution was sprayed on the surface of the aluminum plate at a pressure of 0.6 MPa. In the end, the superhydrophobic PFSC-EDTA composite coatings were fabricated after drying at 180 °C for 90 min.

2.4 $CaCO_3$ scale formation on PFSC and PFSC-EDTA composite coating

The scaling experiments of different coatings were carried out in a static supersaturated calcium carbonate solution, which was prepared by the reaction of calcium nitrate and sodium bicarbonate by Eq. (1)

$$\mathrm{Ca(NO_3)_2 \cdot 4H_2O + 2NaHCO_3 \rightarrow CaCO_3 + 2NaNO_3 + 5H_2O + CO_2 \uparrow} \quad (1)$$

The specific experimental steps were described as follows: Firstly, sodium bicarbonate and calcium nitrate terahydrate were filtered through 0.45-μm membranes, respectively, and then heated to 60 °C in a constant temperature water bath for standby. Secondly, the coated samples (PFSC or PFSC-EDTA) were then immersed vertically into different screw-capped glass bottles containing a supersaturated solution of calcium carbonate. After a certain time interval,

the coated samples were gently removed from the solution, washed with deionized water, and then dried and weighed. At least three samples were tested for each coating, and the average value of the test results was adopted as the scaling amount of the coating sample.

2.5 Characterization

The static contact angles (CAs) of the prepared coatings were measured by contact angle meter (JGW-360A, Chengde City Chenghui Testing Machine Co., Ltd.) with a droplet (5 μL) of deionized water at room temperature. The average CA was obtained from five measurements on different positions of the same specimen. The surface morphology of the coatings before and after scaling were characterized by scanning electron microscopy (SEM; Quanta 200). The functional groups at the prepared coating's surface were detected by Fourier transform infrared (FTIR) spectroscope (Spectrum 2000; PerkinElmer) over the wave number domain from 400 to 4000 cm^{-1}. The X-ray diffraction (XRD; PW3040/60, PANalytical) patterns of the superhydrophobic PFSC and PFSC-EDTA composite coating were obtained in air conditions at 2θ from 10° to 70°. The crystal structure of $CaCO_3$ on different coating surfaces was also studied by XRD. The surface roughness of the coating was measured by a portable surface roughness tester (SJ-210; Mitutoyo). In order to ensure the measurement accuracy, five different positions of the same coating were selected, and the average value of the measurement results was calculated.

3 Results and discussion

3.1 Surface morphology and chemical composition of coatings

The morphology of the as-prepared superhydrophobic PFSC and PFSC-EDTA composite coatings was analyzed by the scanning electron microscope (SEM). As shown in Fig. 2a, the CNTs dispersed uniformly in the grains and grain

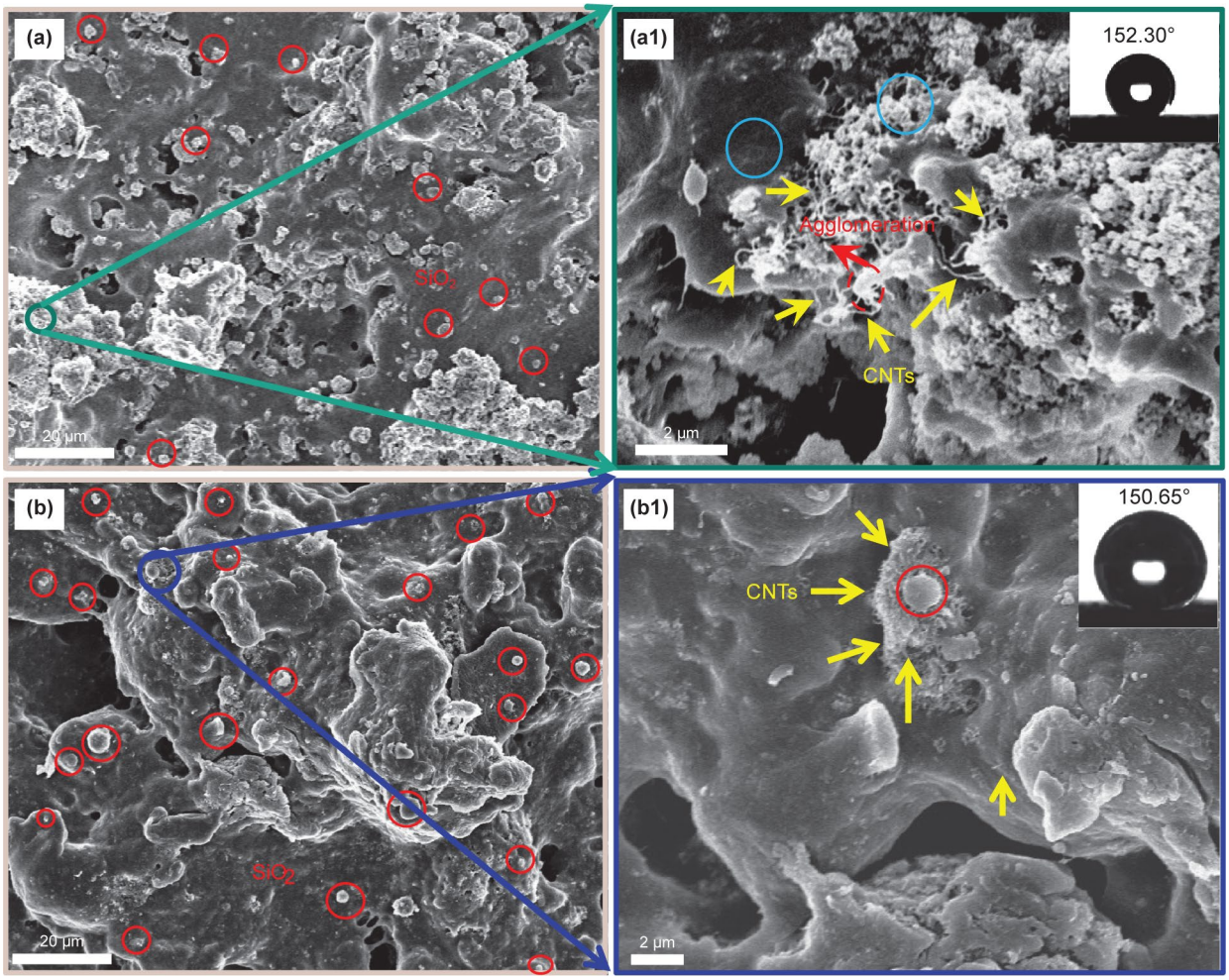

Fig. 2 SEM image of PFSC (**a**, **a1**) and PFSC-EDTA (**b**, **b1**) superhydrophobic composite coating

boundaries of the PFSC composite coating and formed a special network structure. After incorporation with PVDF and FEP, the static water contact angle (WCA) of the PFSC composite coating reached 152.30°. Moreover, the CNTs agglomerated in some regions (Fig. 2a1) owing to the strong van der Waals force, entangled with polymer and nano-SiO_2 grains and formed a special microscopic rough structure (Baghbanzadeh et al. 2016). In addition, there was much of porous, forming a staggered nanonetwork among the CNTs, polymer particles and nano-SiO_2 (Yan et al. 2018), which was benefit for wrapping air in the nanopores structure. For a superhydrophobic coating, the increase in gas–liquid interface proportion (Jagdheesh et al. 2019) will enhance the protection of interface by the air film and further prevent the invasion of corrosive species (Zhang et al. 2018).

Compared with the CNTs in superhydrophobic PFSC composite coating, CNTs-EDTA dispersed more evenly in PFSC-EDTA composite coating (Fig. 2b). Local enlarged image (Fig. 2b1) showed a rough structure centered on SiO_2 and surrounded by CNTs-EDTA formed in the coating. After incorporation with PVDF and FEP, the WCA of PFSC-EDTA composite coating was 150.63° and still showed superhydrophobicity.

The XRD patterns of the pure CNTs, the pure PVDF, the superhydrophobic PFSC composite coating and the PFSC-EDTA composite coating are shown in Fig. 3. The diffraction peaks at 2θ value of 25.7° (002) and 42.8° (100) are the characteristic of CNTs (Fig. 3a) (Gull et al. 2016). The diffraction peaks at 18.3°, 26.5° and 33.0° are attributed to the (020), (021) and (130) α-phase of PVDF, respectively (Fig. 3b). The sharp and strong peak at 19.9° (110) corresponds to β-phase of PVDF (Rajabzadeh et al. 2009). In addition, the diffraction peak at 38.2° is attributed to γ-phase of PVDF and is associated with (131) reflection (Fig. 3b) (You et al. 2012).

Compared with the XRD patterns of the pure CNTs and the pure PVDF, there were new diffraction peaks at 17.8°, 44.7° and 65.1° (Fig. 3c and d) of the superhydrophobic PFSC and PFSC-EDTA composite coating, respectively. The weak peak at 17.8° can be assigned to (100), the α phase reflection of the PVDF. Two strong peaks at 2θ values of 44.7° and 65.1° (100) belong to the aluminum substrate. As a kind of semicrystalline polymer, PVDF exhibits at least four crystalline phases including α, β, γ, and δ, which differ both in physical and in electrical properties. Among them, the α phase PVDF is a monoclinic lattice conformation, which is also the most stable and common crystal structure. The β phase PVDF is the most important crystal structure with an orthorhombic structure. The γ phase PVDF has an orthorhombic lattice, which is usually obtained by annealing α phase crystal at high temperature or isothermal crystallization. The XRD analysis in Fig. 3 showed the PVDF in superhydrophobic PFSC and PFSC-EDTA composite coating including α, β and γ crystalline phases. The EDTA is illegible in XRD for tiny amounts.

The FTIR spectra of pure CNTs, CNTs-EDTA, superhydrophobic PFSC and PFSC-EDTA composite coating were performed (Fig. 4) for analyzing the change of surface functional groups. For the pure CNTs (Fig. 4a), only a flat band can be seen at 3426 cm^{-1} that corresponds to the stretching vibration of –OH (Lu et al. 2016). Compared with pure CNTs, there were three more diffraction bands in the spectrum of CNTs-EDTA (Fig. 4b). Among them, the band at 1624 cm^{-1} is attributed to the vibration of carboxyl–COOH. The small and sharp absorption band at 1394 cm^{-1} corresponds to the in-plane bending vibration of –CH from EDTA. The weak absorption band at

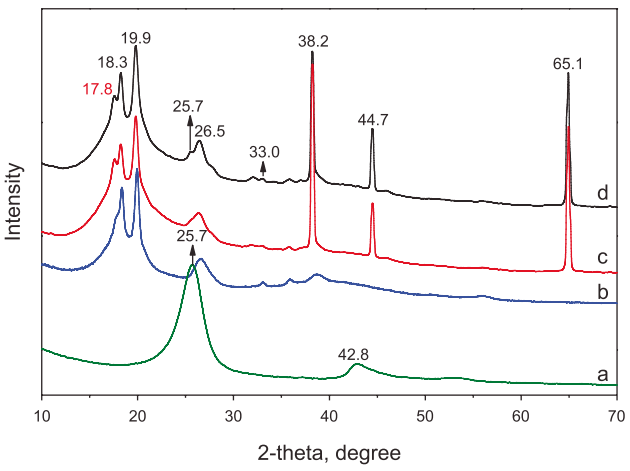

Fig. 3 XRD patterns of the CNTs (**a**), pure PVDF (**b**), as-prepared PFSC coating (**c**) and the PFSC-EDTA coating (**d**)

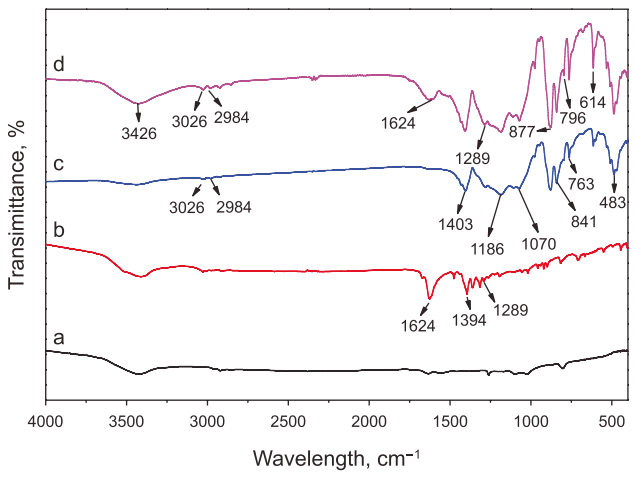

Fig. 4 FTIR spectra of CNTs (**a**), CNTs-EDTA (**b**), PFSC composite coating (**c**) and PFSC-EDTA composite coating (**d**)

1289 cm^{-1} is assigned to the stretching vibration of –CN (Rončević et al. 2019). Combined with the SEM of composite coating (Fig. 2), it can be determined that the EDTA has been successfully loaded on the CNTs. When it comes to the superhydrophobic PFSC (Fig. 4c) and PFSC-EDTA composite coating (Fig. 4d), the absorption bands at 3026 and 2984 cm^{-1} are attributed to the asymmetric stretching vibration of C–H (Ibara et al. 2013), which is independent of the crystalline phase of PVDF. The significant absorption band at 1403 cm^{-1} is related to the bending vibration of $–CH_2$. The strong band at 1186 cm^{-1} is attributed to the bending vibration of $–CF_2$ and $–CF_3$ from the PVDF and the FEP, respectively. The bands at 1070 cm^{-1} of CF_2 bending vibration, 877 cm^{-1} of C–C vibrations, 763 cm^{-1} of $–CH_2$ rocking and 614 cm^{-1} of CF_2 bending imply the existence of α phase PVDF (Rafiee et al. 2010). The band at 841 cm^{-1} of $–CH_2$ bending is correlated with the β phase of PVDF. The specific characteristic band at 483 cm^{-1} represents the CH_2 bending vibration of γ phase PVDF. The FTIR results show that there are three crystal phases PVDF in the superhydrophobic PFSC and PFSC-EDTA composite coating, which is consistent with that of XRD (Fig. 3). The band at about 796 cm^{-1} in PFSC-EDTA composite coating is caused by the symmetric stretching of Si–O from nano-SiO_2. The bands at 1624 and 1289 cm^{-1} can be assigned to the symmetric stretching vibration of –COOH and –CN that come from EDTA, which is the direct evidence for success intercalating of EDTA into the superhydrophobic PFSC-EDTA composite coating (Shi et al. 2018).

3.2 Anti-scaling of the superhydrophobic PFSC and PFSC-EDTA composite coating

In order to illustrate the anti-scaling performance of the superhydrophobic coating, the deposition testing of the $CaCO_3$ scaling at the superhydrophobic PFSC and PFSC-EDTA composite coating surface was carried out. As shown in Fig. 5, the amount of calcium carbonate scaling on the surface of superhydrophobic PFSC and PFSC-EDTA composite coating increased with the immersion time. In comparison with the superhydrophobic PFSC-EDTA composite coating, the superhydrophobic PFSC composite coating had a higher scaling tendency (Fig. 5a). Meanwhile, it experienced a short induction period of scaling for about 8.0 h. After that, the scaling rate of $CaCO_3$ increased sharply. The growth process of $CaCO_3$ scaling consists of two stages: In the first early stage that is from 8 to 96 h, the amount of $CaCO_3$ scaling increased from 0.0393 to 0.3465 mg/cm^2, with an average scaling rate of 0.0035 mg/(cm^2·h). In the second stage from 96 to 192 h, the scaling rate decreased to 0.0004 mg/(cm^2·h), which was probably caused by the reduction in nucleation sites of $CaCO_3$ scaling on the

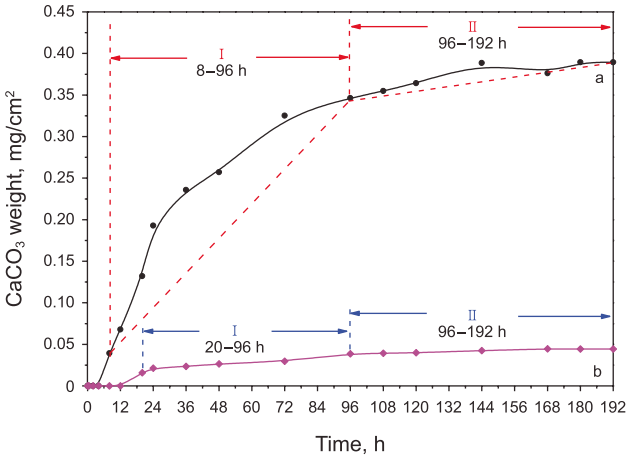

Fig. 5 Deposition rate of $CaCO_3$ scaling at the surface of the superhydrophobic PFSC composite coating (**a**) and superhydrophobic PFSC-EDTA composite coating (**b**)

superhydrophobic PFSC composite coating. In the whole stage of crystal growth from 8 to 192 h, the average scaling rate of $CaCO_3$ on the PFSC composite coating was 0.0019 mg/(cm^2·h).

However, the superhydrophobic PFSC-EDTA composite coating experienced a long $CaCO_3$ scale induction period of about 20 h (Fig. 5b), which was 2.5 times that of superhydrophobic PFSC composite coating. In the first stage from the 20 to the 96th h, the weight of $CaCO_3$ scaling raised from 0.0158 to 0.0387 mg/cm^2 with the average rate of 0.0003 mg/(cm^2·h), which was equivalent to 11.7% of superhydrophobic PFSC composite coating. In the second stage from the 96th h to the 192th h, the average rate of $CaCO_3$ scaling was further reduced to 0.0001 mg/(cm^2·h), which was only 25% of the superhydrophobic PFSC composite coating. In the whole stage of crystal growth from the 20 h to the 192th h, the average scaling rate was 0.0002 mg/(cm^2·h), which was much lower than that of the superhydrophobic PFSC composite coating. The mass of calcium carbonate on the superhydrophobic PFSC-EDTA composite coating surface increased little, which was only 11.4% that of the superhydrophobic PFSC composite coating. The main reason is that the EDTA at the superhydrophobic PFSC-EDTA composite coating interface can chelate the Ca^{2+} in the solution, coupling the coatings' superhydrophobicity, and further prevented the deposition of $CaCO_3$ at the surface.

In addition, the crystal morphology of $CaCO_3$ at different superhydrophobic composite coating surface was characterized by SEM. As shown in Fig. 6a, the cuboid, needlelike, trapezoid prism and irregular block crystals were seen on the surface of superhydrophobic PFSC composite coating for immersion time of 24 h, while for the PFSC-EDTA composite coating in Fig. 6b, the $CaCO_3$ scale at the superhydrophobic surface mainly includes the cube, cuboid and

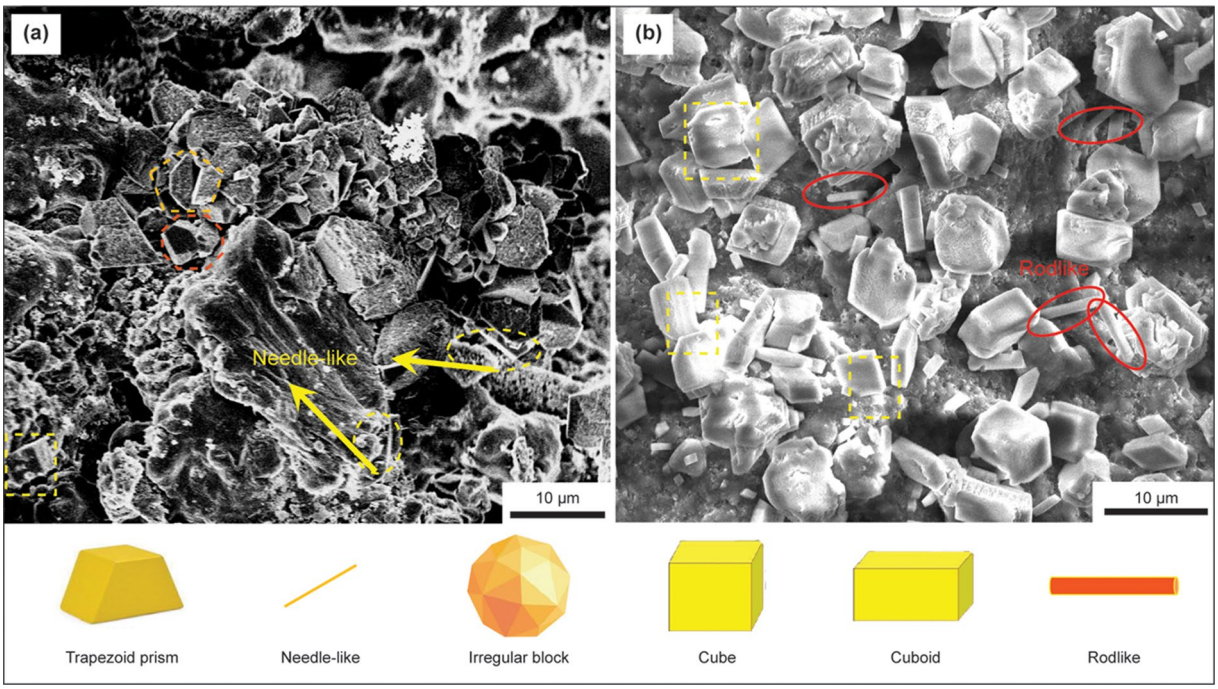

Fig. 6 SEM images of $CaCO_3$ crystallization scaling at the surface of PFSC (**a**) and PFSC-EDTA (**b**) composite coating for immersion time of 24 h

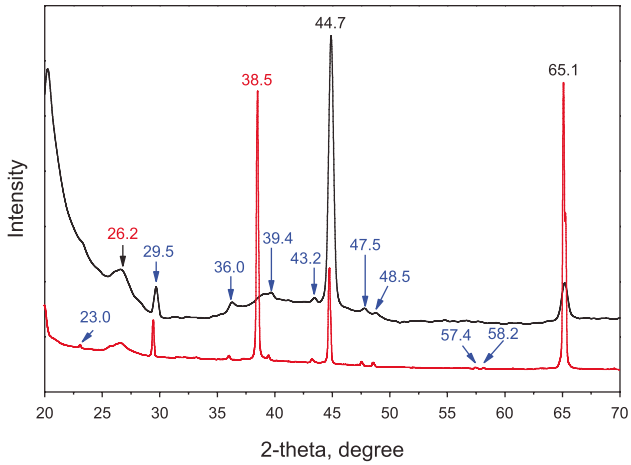

Fig. 7 XRD patterns of $CaCO_3$ scaling on superhydrophobic PFSC (**a**) and superhydrophobic PFSC-EDTA (**b**) composite coating for immersion time of 24 h

rodlike. According to the relevant literature, cube/cuboid, spherical and needle/rodlike structures are typical of calcite, vaterite and aragonite, respectively (Gopi and Subramanian 2012). Therefore, the cubic, cuboid, trapezoidal prism and irregular block crystals are typical crystal forms of calcite (Niu et al. 2014). In the meantime, the calcite is the most stable phase in calcium carbonate crystals. Compared with the crystal morphology of calcite, the needlelike/rodlike crystals at the surface of the superhydrophobic PFSC and superhydrophobic PFSC-EDTA composite coatings are the aragonite $CaCO_3$.

XRD results of calcium carbonate scale at the surface of superhydrophobic PFSC and PFSC-EDTA composite coating after 24-h $CaCO_3$ deposition are shown in Fig. 7. The characteristic peaks at 44.6 and 65.1° belonged to the aluminum substrate. The diffraction peaks of calcite appeared at 23.0 (012), 29.5 (104), 36.0 (110), 39.4 (113), 43.2 (202), 47.5 (024), 48.5 (116), 57.4 (122) and 58.2 (1010). In addition, the aragonite also existed at the surface of superhydrophobic PFSC and PFSC-EDTA composite coating. The characteristic peaks of aragonite appeared at 26.2 and 38.5° indexing to (111) and (130), respectively. Results showed that the calcite and aragonite $CaCO_3$ crystals were all formed at the surface of the superhydrophobic PFSC and PFSC-EDTA composite coating and with different peak intensity. For the superhydrophobic PFSC composite coating (Fig. 7a), the peak intensity of calcite at 29.5° and aragonite at 26.2° was all weak. When it comes to the PFSC-EDTA composite coating (Fig. 7b), the strong peak at 38.5° of aragonite can be seen clearly and the weakness peak at 29.5° may be a sign of relative low content of calcite $CaCO_3$ crystals. The results of XRD (Fig. 7) and SEM (Fig. 6) analysis of $CaCO_3$ scale showed that the addition of organic chelating agent EDTA in the superhydrophobic PFSC-EDTA composite coating

Table 1 Molar fraction of $CaCO_3$ polymorphs deposited on the surface of different coatings

Superhydrophobic composite coatings	Molar fraction, %	
	Calcite	Aragonite
PFSC	69.3	30.7
PFSC-EDTA	4.4	95.6

induced the formation of aragonite crystal and significantly changed the morphology of $CaCO_3$ crystal.

The molar fraction of aragonite and calcite can be calculated from X-ray diffraction data by Eqs. (2) and (3) (Liu et al. 2011),

$$X_A = \frac{I_A}{I_A + 0.41I_C} \tag{2}$$

$$X_C = \frac{I_C}{2.44I_A + I_C} \tag{3}$$

where X is the molar fraction of $CaCO_3$ polymorphs, the subscripts "A" and "C" represent aragonite and calcite, respectively. I_A and I_C indicate the intensity of the main peak of aragonite at 38.5° and calcite at 29.5°, respectively. As shown in Table 1, the molar fraction of calcite and aragonite in $CaCO_3$ scaling that deposited at the surface of the superhydrophobic PFSC composite coating is 69.3 and 30.7%, that is, calcite is the principal constituent of the $CaCO_3$ scaling. For the superhydrophobic PFSC-EDTA composite coating, the aragonite becomes the main part with content of 95.6% and calcite of 4.4%. As we know, the calcite is the most stable one in the three crystals: $CaCO_3$ of calcite, aragonite and vaterite (Gopi and Subramanian 2012). Results of the PFSC-EDTA composite coating show that the existence of organic chelating agent EDTA induced the formation of aragonite crystals (Gopi et al. 2015); the more the aragonite or vaterite in the scale, the better the anti-scaling performance (Li et al. 2015; Ge et al. 2016), which is benefit for preventing the deposition of $CaCO_3$ at the surface. Therefore, the addition of organic chelating agent EDTA has a significant effect on the anti-scaling performance of the superhydrophobic PFSC-EDTA composite coating.

3.3 Effect of the EDTA on anti-scaling of superhydrophobic composite coating

The adhesion of $CaCO_3$ scaling on the superhydrophobic composite coating can be analyzed by the surface energy, which is the direct measurement of the interfacial attractive forces. For the superhydrophobic coating, the surface roughness is also another important parameter for anti-scaling performance. According to the static CAs of deionized water and ethylene glycol, the surface free energy of different superhydrophobic coating can be calculated by a series of equations (Young 1805):

$$\gamma_L \cos\theta = \gamma_L - \gamma_{SL} \tag{4}$$

$$\gamma_S = \gamma_S^{LW} - \gamma_S^{AB} \tag{5}$$

$$\gamma_L = \gamma_L^{LW} - \gamma_L^{AB} \tag{6}$$

$$\gamma_L(1 + \cos\theta) = 2\left(\gamma_S^{LW}\gamma_L^{LW}\right)^{0.5} + 2\left(\gamma_S^{AB}\gamma_L^{AB}\right)^{0.5} \tag{7}$$

where θ is the static CA of pure liquid on solid surface, γ_S and γ_L are the surface free energy of solid and the surface tension of liquid–vapor, respectively. γ_{SL} is the solid–liquid interface energy. The homologous surface tension components of deionized water and ethylene glycol are shown in Table S1. The results obtained from measurement and calculation of CAs and surface free energy of different superhydrophobic coatings are shown in Table S2. In addition, the surface roughness of superhydrophobic composite coatings was measured before $CaCO_3$ scaling test (Table S3). R_a is the arithmetic average deviation (Rahman et al. 2011):

$$R_a = \frac{1}{l}\int_0^l |Z(x)|\mathrm{d}x \tag{8}$$

where $Z(x)$ and l represent the sampling height and the length of the assessed profile at an arbitrary point x, respectively. During the $CaCO_3$ scaling test, the scanning length and the scanning speed were 5.0 mm and 0.25 mm·s^{-1}, respectively.

As shown in Fig. 8, the surface free energy of the superhydrophobic PFSC and PFSC-EDTA composite coating is 0.40 (Fig. 8a) and 0.95 mJ/m^2 (Fig. 8b), respectively, that is consistent with the rule of the lower the surface free

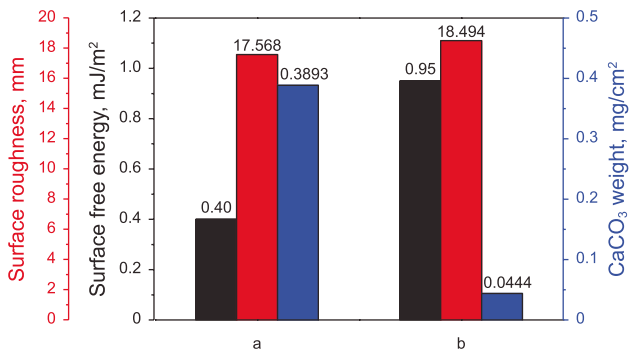

Fig. 8 Surface free energy, surface roughness and $CaCO_3$ weight for 192-h immersion of superhydrophobic PFSC (**a**) and PFSC-EDTA (**b**) composite coating

energy, the better the anti-scaling performance of the coating (Azim et al. 2014; Förster and Bohnet 1999; Muller-Steinhagen and Zhao 1997). On the one hand, the addition of EDTA in the fabrication of superhydrophobic PFSC-EDTA composite coating would increase the surface free energy and decrease the scaling rate of calcium carbonate only to 11.4% (0.0444 mg/cm^2, Fig. 8b) that of the superhydrophobic PFSC composite coating (0.3893 mg/cm^2, Fig. 8a). On the other hand, the surface roughness of the superhydrophobic PFSC-EDTA composite coating is 18.494 μm, which is a little higher than 17.568 μm that of the superhydrophobic PFSC composite coating owing to the rough surface of SiO_2-centric and CNTs-EDTA-surrounded multilevel micro–nanostructure as shown in SEM (Fig. 2). That is to say both the surface free energy and roughness are responsible for the anti-scaling of the superhydrophobic coating, which is also consistent with the previous study (Qian et al. 2020). Furthermore, in terms of the chemical composition of the coating, the biggest difference between the superhydrophobic PFSC and PFSC-EDTA composite coating is whether there is the organic chelating agent EDTA. As a good complexing agent of Ca^{2+}, EDTA could help reducing the number of free calcium ions in the solution, which also decreases the nucleation driving force of calcium carbonate formation (Meng and Park 2014). Consequently, the EDTA at the interface of coating and solution can still play a certain role on anti-scaling by chelating the free Ca^{2+} and prompting good $CaCO_3$ deposition prevention performance of superhydrophobic PFSC-EDTA composite coating. The SEM of calcium carbonate scale at the surface of superhydrophobic PFSC (Fig. 6a) and superhydrophobic PFSC-EDTA (Fig. 6b) composite coating identified the obvious influence of EDTA to the crystal morphology of $CaCO_3$, which is also consistent with others' result (Gopi and Subramanian 2012).

3.4 Anti-scaling mechanistic of the superhydrophobic PFSC-EDTA composite coating

As discussed, the deposition of $CaCO_3$ at the surface of the superhydrophobic coating was influenced by the air film that retains between the solution and the coating. For the superhydrophobic PFSC composite coating, although the air film can be retained at the interface of supersaturated $CaCO_3$ solution and coating (Fig. 9a), still a number of $CaCO_3$ scales can be formed owing to the poor superhydrophobic stability under the water (Fig. 9b). As for the superhydrophobic PFSC-EDTA composite coating, the most important factor influencing the anti-scaling behavior is the organic chelating agent EDTA, followed by the surface roughness, and finally the surface free energy. For the superhydrophobic PFSC and PFSC-EDTA composite coating, a porous and rough structure was formed among CNTs, nano-SiO_2 and PVDF (Fig. 2a) (Latthe et al. 2019), which is also the prerequisite condition for the formation of superhydrophobic coating (Tretheway and Meinhart 2004). Together with the high strength of CNTs, the porous structure can be maintained well and contributed for the stability of the air film (Fig. 9a).

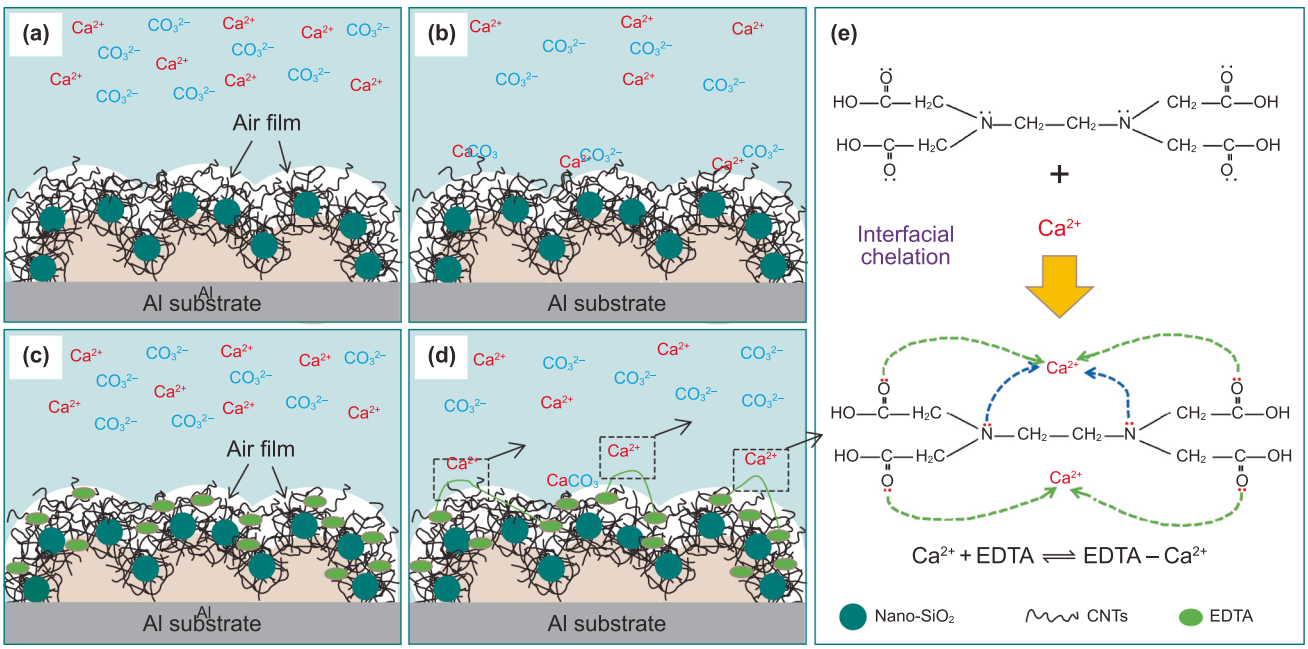

Fig. 9 Schematic diagram of $CaCO_3$ scaling formation at the surface of superhydrophobic PFSC (**a**, **b**) and PFSC-EDTA (**c**, **d**) composite coating, and the interfacial chelation between Ca^{2+} and EDTA of superhydrophobic PFSC-EDTA composite coating (**e**)

In addition, the low surface energy and tackling effect of CNTs can effectively prevent the adhesion of $CaCO_3$ on the coating surface (Fig. 9b) (Qian et al. 2020).

After the CNTs were impregnated with EDTA, the anti-scaling of the superhydrophobic PFSC-EDTA composite coating has been greatly improved. As shown in Fig. 9c, the superhydrophobicity of the PFSC-EDTA composite coating assures the stable existence of air film at the interface of the $CaCO_3$ solution and coating. Owing to the enhancements of CNTs at the interface, the EDTA dispersed in the gaps among the fillers of CNTs, nano-SiO_2 and the polymer of PVDF. The SiO_2-centric and CNTs-EDTA-surrounded rough structure would help to wrap air and form a thick air film and increase the proportion of gas–liquid interface (Jagdheesh et al. 2019), which could reduce the contact area between solid and liquid and hinder the nucleation and growth of calcium carbonate on the coating surface (Fig. 9c). In addition, the rough structure of the PFSC-EDTA composite coating surface is good for wrapping the air and maintaining the air film stability (Fig. 9c) (Qian et al. 2020). The most important point is the Ca^{2+} ions that from the supersaturated $CaCO_3$ solution can be chelated by the EDTA at the solution/coating interface, which would reduce the contact chances of Ca^{2+} ions with CO_3^{2-} to form calcium carbonate (Fig. 9d). The interfacial chelation between EDTA and Ca^{2+} ions at the interface is shown in Fig. 9e; it can be seen that the two amino nitrogen and four carboxyl oxygen in the EDTA molecular could coordinate with calcium ion and form the intermediated EDTA-Ca^{2+} chelate that also had inhibition of calcite scaling (Zhu et al. 2021). All in all, the synergistic effect of coatings' superhydrophobicity that depending on the surface roughness and surface free energy and the interfacial chelation of EDTA and Ca^{2+} at the supersaturated $CaCO_3$ solution/coating interface tremendously enhance the anti-scaling of the superhydrophobic PFSC-EDTA composite coating. This work of superhydrophobic PFSC-EDTA composite coating incorporating the interfacial chelation at the interface of solution and coating provides a new idea and method for water scale inhibition for wastewater in oilfield and corresponding industries.

4 Conclusions

In this article, a novel EDTA-incorporated CNTs (CNTs-EDTA) and nano-SiO_2 filling PVDF/FEP superhydrophobic coating was fabricated and the corresponding anti-scaling performance has been investigated. The incorporation of EDTA to the CNTs played an important role in fabricating a SiO_2-centric and CNTs-EDTA-surrounded multilevel micro–nanostructure in the superhydrophobic PFSC-EDTA composite coating. The synergistic effect of surface roughness and the low surface free energy decided the good superhydrophobicity, which is benefit for maintaining the air film under the water and the stability of the superhydrophobic surfaces. The most important of all is that the interfacial chelation of EDTA and Ca^{2+} at the supersaturated $CaCO_3$ solution and superhydrophobic PFSC-EDTA coating interface further enhanced the coating's anti-scaling. Results showed that the amount of $CaCO_3$ scaling on the superhydrophobic PFSC-EDTA composite coating after 192-h immersion into the supersaturated $CaCO_3$ solution was 0.0444 mg/cm^2, which is only 11.4% that of the superhydrophobic PFSC coating. This research provides a new method of fabrication for the anti-scaling surface by introducing the scale inhibition at the interface of superhydrophobic coating, which is the development and optimization of traditional way of scale prevention in petroleum industry.

Supplementary Information The online version contains supplementary material available at (https://doi.org/10.1007/s12182-021-00558-x).

Acknowledgements The research was financially supported by the National Science Foundation for Distinguished Young Scholars of China (Grant No. 51925403), the Major Research Plan of National Natural Science Foundation of China (Grant No. 91934302) and the National Science Foundation of China (21676052, 21606042).

References

Azimi G, Cui Y, Sabanska A, Varanasi KK. Scale-resistant surfaces: fundamental studies of the effect of surface energy on reducing scale formation. Appl Surf Sci. 2014;313:591–9. https://doi.org/10.1016/j.apsusc.2014.06.028.

Baghbanzadeh M, Rana D, Lan CQ, Matsuura T. Effects of inorganic nano-additives on properties and performance of polymeric membranes in water treatment. Sep Purif Rev. 2016;45:141–67. https://doi.org/10.1080/15422119.2015.1068806.

Förster M, Bohnet M. Influence of the interfacial free energy crystal/heat transfer surface on the induction period during fouling. Int J Therm Sci. 1999;38:944–54. https://doi.org/10.1016/s1290-0729(99)00102-7.

Ge JJ, Wang Y, Zhang GC, Jiang P, Sun MQ. Investigation of scale inhibition mechanisms based on the effect of HEDP on surface charge of calcium carbonate. Tenside Surfactants Deterg. 2016;3:29–36. https://doi.org/10.3139/113.110407.

Gopi SP, Subramanian VK. Polymorphism in $CaCO_3$-effect of temperature under the influence of EDTA (di sodium salt). Desalination. 2012;297:38–47. https://doi.org/10.1016/j.desal.2012.04.015.

Gopi SP, Subramanian VK, Palanisamy K. Synergistic effect of EDTA and HEDP on the crystal growth, polymorphism, and morphology of $CaCO_3$. Ind Eng Chem Res. 2015;54:3618–25. https://doi.org/10.1021/ie5034039.

Gull N, Khan SM, Islam A, Zia S, Shafiq M, Sabir A, Munawar MA, Butt MTZ, Jamil T. Effect of different oxidants on polyaniline/single-walled carbon nanotubes composites synthesized via ultrasonically initiated in situ chemical polymerization. Mater Chem Phys. 2016;172:39–46. https://doi.org/10.1016/j.matchemphys.2015.12.048.

Ibara A, Miyaji H, Fugetsu B, Nishida E, Kawanami M. Osteoconductivity and biodegradability of collagen scaffold coated with nano-β-TCP and fibroblast growth factor 2. J Nanomater. 2013;10:639502. https://doi.org/10.1155/2013/639502.

Jagdheesh R, Hauschwitz P, Muzik J, Brajer J, Rostohar D, Jiříček P, Kopeček J, Moceka T. Non-fluorinated superhydrophobic Al7075 aerospace alloy by ps laser processing. Appl Surf Sci. 2019;493:287–93. https://doi.org/10.1016/j.apsusc.2019.07.035.

Kan AT, Dai ZY, Tomson MB. The state of the art in scale inhibitor squeeze treatment. Pet Sci. 2020. https://doi.org/10.1007/s12182-020-00497-z.

Khormali A, Petrakov DG. Laboratory investigation of a new scale inhibitor for preventing calcium carbonate precipitation in oil reservoirs and production equipment. Pet Sci. 2016;13:320–7. https://doi.org/10.1007/s12182-016-0085-6.

Latthe SS, Sutar RS, Kodag VS, Bhosale AK, Kumar AM, Sadasivuni KK, Xing RM, Liu SH. Self-cleaning superhydrophobic coatings: potential industrial applications. Prog Org Coat. 2019;128:52–8. https://doi.org/10.1016/j.porgcoat.2018.12.008.

Li X, Gao B, Yue Q, Ma D, Rong H, Zhao P, Teng P. Effect of six kinds of scale inhibitors on calcium carbonate precipitation in high salinity wastewater at high temperatures. J Environ Sci. 2015;29:124–30. https://doi.org/10.1016/j.jes.2014.09.027.

Liu Y, Zou Y, Zhao L, Liu W, Cheng L. Investigation of adhesion of $CaCO_3$ crystalline fouling on stainless steel surfaces with different roughness. Int Commun Heat Mass Transf. 2011;38:730–3. https://doi.org/10.1016/j.icheatmasstransfer.2011.04.003.

Liu Y, Chen S, Guan B, Xu P. Layout optimization of large-scale oil-gas gathering system based on combined optimization strategy. Neurocomputing. 2019;332:159–83. https://doi.org/10.1016/j.neucom.2018.12.021.

Lu Y, Jiang B, Fang L, Ling F, Gao J, Wu F, Zhang X. High performance NiFe layered double hydroxide for methyl orange dye and Cr(VI) adsorption. Chemosphere. 2016;152:415–22. https://doi.org/10.1016/j.chemosphere.2016.03.015.

Meng LY, Park SJ. Superhydrophobic carbon-based materials: a review of synthesis, structure, and applications. Carbon Lett. 2014;15:89–104. https://doi.org/10.5714/CL.2014.15.2.089.

Mpelwa M, Tang SF. State of the art of synthetic threshold scale inhibitors for mineral scaling in the petroleum industry: a review. Pet Sci. 2019;16:830–49. https://doi.org/10.1007/s12182-019-0299-5.

Muller-Steinhagen H, Zhao Q. Investigation of low fouling surface alloys made by ion implantation technology. Chem Eng Sci. 1997;52:3321–32. https://doi.org/10.1016/S0009-2509(97)00162-0.

Niu T, Xu J, Huang J. Growth of aragonite phase calcium carbonate on the surface of a titania-modified filter paper. CrystEngComm. 2014;16:2424–31. https://doi.org/10.1039/c3ce42322k.

Qian H, Zhu Y, Wang H, Song H, Wang C, Liu Z, Li H. Preparation and anti-scaling performance of superhydrophobic PPS/PTFE composite coating. Ind Eng Chem Res. 2017;56:12663–71. https://doi.org/10.1021/acs.iecr.7b03975.

Qian H, Zhu M, Song H, Wang H, Wang C. Anti-scaling of superhydrophobic poly(vinylidene fluoride) composite coating: tackling effect of carbon nanotubes. Prog Org Coat. 2020;142:105566. https://doi.org/10.1016/j.porgcoat.2020.105566.

Rafiee MA, Lu W, Thomas AV, Zandiatashbar A, Rafiee J, Tour JM, Koratkar NA. Graphene nanoribbon composites. ACS Nano. 2010;4:7415–20. https://doi.org/10.1021/nn102529n.

Rahman MM, Khan MAR, Kadirgama K, Noor MM, Bakar RA. Experimental investigation into electrical discharge machining of stainless steel 304. J Appl Sci. 2011;11:549–54. https://doi.org/10.3923/jas.2011.549.554.

Rajabzadeh S, Maruyama T, Ohmukai Y, Sotani T, Matsuyama H. Preparation of PVDF/PMMA blend hollow fiber membrane via thermally induced phase separation (TIPS) method. Sep Purif Technol. 2009;66:76–83. https://doi.org/10.1016/j.seppur.2008.11.021.

Rončević S, Nemet I, Ferri TZ, Matković-Čalogović D. Characterization of nzvi nanoparticles functionalized by edta and dipicolinic acid: a comparative study of metal ion removal from aqueous solutions. RSC Adv. 2019;9:31043–51. https://doi.org/10.1039/C9RA04831F.

Shi Y, Zhang T, Ren H, Kruse A, Cui R. Polyethylene imine modified hydrochar adsorption for chromium (VI) and nickel (II) removal from aqueous solution. Bioresour Technol. 2018;247:370–9. https://doi.org/10.1016/j.biortech.2017.09.107.

Tretheway DC, Meinhart CD. A generating mechanism for apparent fluid slip in hydrophobic microchannels. Phys Fluids. 2004;16:1509–15. https://doi.org/10.1063/1.2361313.

Vazirian MM, Charpentier TVJ, Penna MDO, Neville A. Surface inorganic scale formation in oil and gas industry: as adhesion and deposition processes. J Petrol Sci Eng. 2016;137:22–32. https://doi.org/10.1016/j.petrol.2015.11.005.

Wang Z, Bai Y, Zhang H, Liu Y. Investigation on gelation nucleation kinetics of waxy crude oil emulsions by their thermal behavior. J Petrol Sci Eng. 2019a;181:106230. https://doi.org/10.1016/j.petrol.2019.106230.

Wang Z, Lin X, Yu T, Zhou N, Zhong H, Zhu J. Formation and rupture mechanisms of visco-elastic interfacial films in polymer-stabilized emulsions. J Dispers Sci Technol. 2019b;40(4):612–26. https://doi.org/10.1080/01932691.2018.1478303.

Yan KK, Jiao L, Lin S, Lu X, Zhang L. Superhydrophobic electrospun nanofiber membrane coated by carbon nanotubes network for membrane distillation. Desalination. 2018;437:26–33. https://doi.org/10.1016/j.desal.2018.02.020.

You J, Dong W, Zhao L, Cao X, Qiu J, Sheng W, Li Y. Crystal orientation behavior and shape-memory performance of poly(vinylidene fluoride)/acrylic copolymer blends. J Phys Chem B. 2012;116:1256–64. https://doi.org/10.1021/jp209116u.

Young T. An essay on the cohesion of fluids. Philos Trans R Soc Lond. 1805;95:65–87. https://doi.org/10.1098/rstl.1805.0005.

Zhang X, Zhi D, Sun L, Zhao Y, Tiwari MK, Carmalt CJ, Parkin IP, Lu Y. Super-durable, non-fluorinated superhydrophobic free-standing items. J Mater Chem A. 2018;6:357–62.

Zhu Y, Li H, Zhu M, Wang H, Li Z. Dynamic and active antiscaling via scale inhibitor pre-stored superhydrophobic coating. Chem Eng J. 2021;403:126467. https://doi.org/10.1016/j.cej.2020.126467.